with the condition

$$\ln \rho_s < \lambda_{tot}/4k_BT \quad (17)$$

Aviram has discussed the theoretical possibility of constructing logic gates by suitable molecular switch circuits. It is of interest to note the restraints on the molecular parameters required to match specifications of current chip technology. In the absence of an applied field ($F_s = 0$) the memory retention time τ_{mem} is given by $\tau_{mem} = \tau_0 \exp(\lambda/4k_BT)$: the ratio of the memory retention time to the minimum switching time τ_0 depends sensitively on both the electronic coupling J and the reorganization energy. For current dynamic RAM operation values of the data retention and switching times τ_{mem} and τ_0 on the order of 8 ms and 70 ns, respectively, with ratio 10^5, are typical. At 300 K, the molecular requirements to match this are $J = 0.3 \times 10^{-4}$ eV and $\lambda = 0.8$ eV. For static or ECL RAM operation, typical specifications are $\tau_{mem} = 10$ yr (3×10^7 s), with τ_0 in the range 2-25 ns. At the molecular level at 300 K these would be matched by $J = 2.4$-0.67×10^{-4} eV and $\lambda = 2.5$-2.4 eV, respectively: these molecular specifications for J and λ are reasonably and easily met by suitable bridge design, but very high critical field strengths are required for fast switching times because of the large value of λ. Lowering the temperature assists the operation of these devices by slightly reducing τ_0 and dramatically increasing τ_{mem}. In an alternative architecture, logic gates could be constructed from combinations of these "molecular gates" which would, like modern electronic gates, contain high feedback loops. These feedback loops would ensure memory retention at modest λ while permitting fast switching times.

For the isolated model system considered above, only the internal contribution to the reorganization energy has been explicitly considered. If the system is transferred to an ionic or ionizing environment, however, coupling to ionic or solvent modes will make a large contribution to λ_{tot}: for the anthracene/anthracene$^-$ pair at close contact distance in acetonitrile, for example, this is estimated to be 1 eV,[30] very much larger than that estimated for coupling to internal modes. On the other hand, in one of the configurations envisaged by Aviram for molecules of the type of Figure 2, the molecules are linked into a presumably metallic grid: in this case, most of the contribution to λ will still arise from coupling to internal modes. Calculation of the relevant internal coupling constants g_l would be required in order to estimate the switching and retention times for these proposed systems. It should also be noted that the effective two-level Hamiltonian of the type considered above is only appropriate in the case that there are no resonances or near resonances with bridge states: where this is not the case, the critical field and dynamical field parameters will have a less simple relationship to geometry and reorganization energy.[8]

Acknowledgment. J.R.R. acknowledges award of a Senior Research Fellowship by the Australian Research Council, and A.T.W. acknowledges receipt of a Commonwealth Postgraduate Award.

Vibronic Coupling Model for the Calculation of Mixed-Valence Line Shapes: A New Look at the Creutz-Taube Ion

Susan B. Piepho

Contribution from the Department of Chemistry, Sweet Briar College, Sweet Briar, Virginia 24595. *Received October 16, 1989*

Abstract: The vibronic coupling model we described in a recent paper is applied to the Creutz-Taube (C-T) ion, (μ-pyrazine)bis(pentaammineruthenium)(5+). We present calculations of the band shape and g values of the C-T ion using a molecular orbital basis. Parameters are estimated from experimental data. The analysis supports the conclusion that the ion is a delocalized mixed-valence system with the mixed-valence band arising from the $b_{2g}^*(d,\pi) \rightarrow b_{3u}(d,\pi^*)$ excitation. Both π^* back-bonding in the $b_{3u}(d,\pi^*)$ MO and π bonding in the $b_{2g}^*(d,\pi)$ MO are significant. The π bonding that gives rise to the $b_{2g}^*(d,\pi)$ MO is the origin of the large rhombic splitting parameter used to fit the g values in crystal field analyses of the C-T ESR spectrum. We show how magnitudes of the orbital vibronic constants (OVC), which govern vibronic coupling, are related the MO's involved. We argue that the band shape of the C-T mixed-valence band arises primarily from coupling to a molecular mode whose motion connects the bond lengths before and after the $b_{2g}^*(d,\pi) \rightarrow b_{3u}(d,\pi^*)$ excitation. The narrow width of the band is explained with reference to the OVC involved. The effect of vibronic parameters on the g values is discussed. While the analysis in the paper is directed specifically at the C-T ion, the methods used are presented in a general form and can easily be applied to other ions.

I. Introduction

In a recent paper[1] we developed a simplified vibronic coupling model for mixed-valence systems. Here we follow section VII of ref 1 and apply the model to a real system, the Creutz-Taube (C-T) ion,[2] (μ-pyrazine)bis(pentaammineruthenium)(5+). We choose this ion as an initial system since it has been studied in more detail, both experimentally and theoretically, than other mixed-valence ions.

Like the PKS model,[3] this new model[1] provides explicit vibronic eigenvalues and eigenfunctions with which the absorption profile may be obtained for the full range of mixed-valence systems from the localized (class II) to the delocalized (class III). It differs from the PKS model in that *multicenter* vibrations (such as the A-B stretch in a simple A-B dimer) play an important role, while the PKS model includes vibronic coupling *only* to linear combinations of vibrations *localized on the metal ion centers*. We have shown[1] that coupling to *both* types of vibrations is involved in even the simplest mixed-valence systems. A molecular orbital basis is used (as in the work of Ondrechen et al.[4]) rather than the valence-bond type basis of the PKS model. We also showed

(1) Piepho, S. B. *J. Am. Chem. Soc.* **1988**, *110*, 6319-6326.
(2) (a) Creutz, C.; Taube, H. *J. Am. Chem. Soc.* **1969**, *91*, 3988. (b) Creutz, C.; Taube, H. *J. Am. Chem. Soc.* **1973**, *95*, 1086.
(3) Piepho, S. B.; Krausz, E. R.; Schatz, P. N. *J. Am. Chem. Soc.* **1978**, *100*, 2996-3005.
(4) (a) Root, L. J.; Ondrechen, M. J. *Chem. Phys. Lett.* **1982**, *93*, 421-424. (b) Ondrechen, M. J.; Ko, J.; Root, L. J. *J. Phys. Chem.* **1984**, *88*, 5919-5923. (c) Ko, J.; Ondrechen, M. J. *Chem. Phys. Lett.* **1984**, *112*, 507-512. (d) Ko, J.; Ondrechen, M. J. *J. Am. Chem. Soc.* **1985**, *107*, 6161-6167. (e) Ko, J.; Zhang, L.-T.; Ondrechen, M. J. *J. Am. Chem. Soc.* **1986**, *108*, 1712-1713. (f) Zhang, L.-T.; Ko, J.; Ondrechen, M. J. *J. Am. Chem. Soc.* **1987**, *109*, 1666-1671. (g) Ondrechen, M. J.; Ko, J.; Zhang, L.-T. *J. Am. Chem. Soc.* **1987**, *109*, 1672-1676. (h) Zhang, L.-T.; Ko, J.; Ondrechen, M. J. *J. Phys. Chem.* **1989**, *93*, 3030-3034.

0002-7863/90/1512-4197$02.50/0

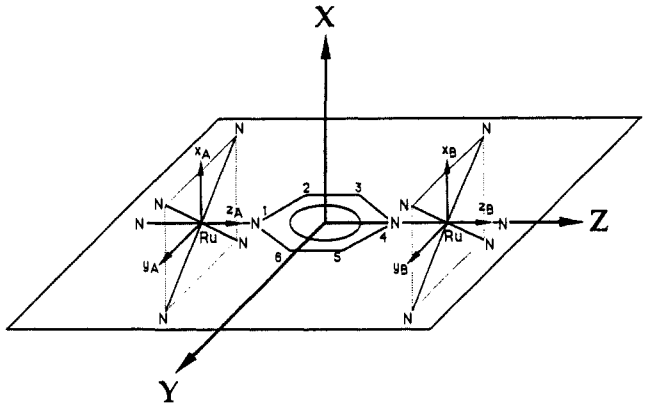

Figure 1. Coordinate systems and structure of the C–T ion. The pyrazine ring is in the YZ plane. X, x_A, and x_B are parallel as are Y, y_A, and y_B, and Z, z_A, and z_B. The ammonia hydrogens have been omitted for clarity.

how vibronic coupling in mixed-valence compounds is similar to vibronic coupling in more "conventional" molecules and how Bersuker's orbital vibronic constants (OVC)[5] may be used to parameterize this coupling.[1]

In the present paper we use the method of ref 1 to calculate both the absorption profile and the g values for the C–T ion. We show how spectroscopic and other experimental data may be used to estimate electronic parameters and how estimates may also be made of the OVC. Our analysis shows the interdependence of vibronic and MO effects. The C–T ion clearly falls toward the delocalized extreme of mixed-valence systems. However, we present our analysis in such a way that our method can be applied to the full range of mixed-valence systems.

II. Simple Model for the Creutz–Taube Ion

Figure 1 gives the coordinate system and structure of the Creutz–Taube ion. The symmetry of the ion is approximately (or in some hosts exactly) D_{2h}. Each Ru is surrounded by five ammonia nitrogens and one pyrazine nitrogen. While the exact Ru site symmetry is C_{2v}, the Ru centers may be viewed as distorted octahedra.

A schematic MO diagram for the complex is given in Figure 2. Only the orbitals that figure prominently in our discussion are included. The average Ru valence is 2.5 so the two Ru centers contribute a total of 11 4d electrons to the complex. In O_h these are t_{2g} electrons, but in C_{2v} the Ru 4d orbitals transform as a_1, b_2, and b_3. More explicitly, our Ru basis orbitals are

$$|a_1(\mathrm{Ru})\rangle = d_{x^2-y^2}$$
$$|b_2(\mathrm{Ru})\rangle = d_{xz}$$
$$|b_3(\mathrm{Ru})\rangle = -id_{yz} \qquad (1)$$

We label the two Ru centers A and B. From these orbitals on each Ru, two D_{2h} metal (d) symmetry orbitals can be constructed that have the proper symmetry to interact with π and π^* orbitals from the pyrazine bridge

$$|b_{2g}(\mathrm{d})\rangle = (1/\sqrt{2})(|b_2(\mathrm{A})\rangle + |b_2(\mathrm{B})\rangle)$$
$$|b_{3u}(\mathrm{d})\rangle = (1/\sqrt{2})(|b_2(\mathrm{A})\rangle - |b_2(\mathrm{B})\rangle) \qquad (2)$$

and four that *do not*

$$|a_g(\mathrm{d})\rangle = (1/\sqrt{2})(|a_1(\mathrm{A})\rangle + |a_1(\mathrm{B})\rangle)$$
$$|b_{1u}(\mathrm{d})\rangle = (1/\sqrt{2})(|a_1(\mathrm{A})\rangle - |a_1(\mathrm{B})\rangle)$$
$$|b_{3g}(\mathrm{d})\rangle = (1/\sqrt{2})(|b_3(\mathrm{A})\rangle + |b_3(\mathrm{B})\rangle)$$
$$|b_{2u}(\mathrm{d})\rangle = (1/\sqrt{2})(|b_3(\mathrm{A})\rangle - |b_3(\mathrm{B})\rangle) \qquad (3)$$

Pyrazine has a π and a π^* orbital of b_{2g} symmetry and a π and

(5) Bersuker, I. B. *The Jahn-Teller Effect and Vibronic Interactions in Modern Chemistry*; Plenum: New York, 1984.

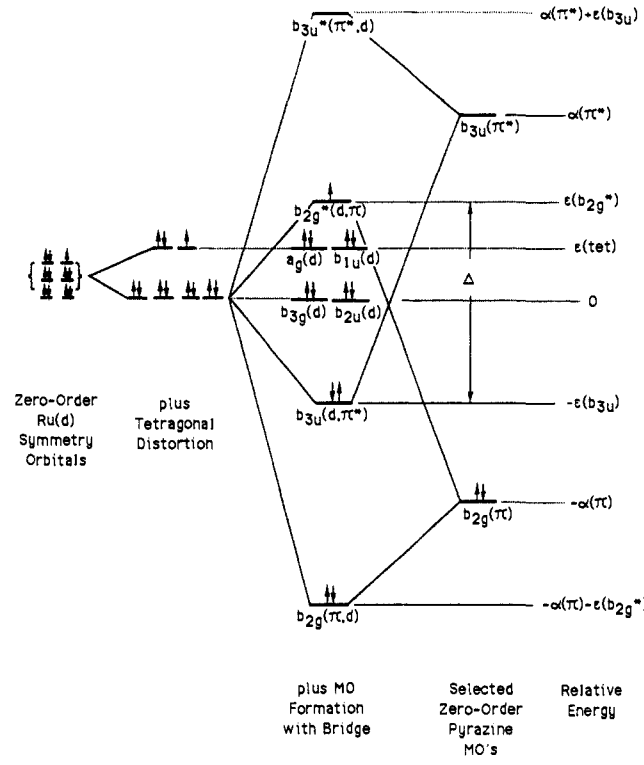

Figure 2. Schematic MO diagram for the C–T ion.

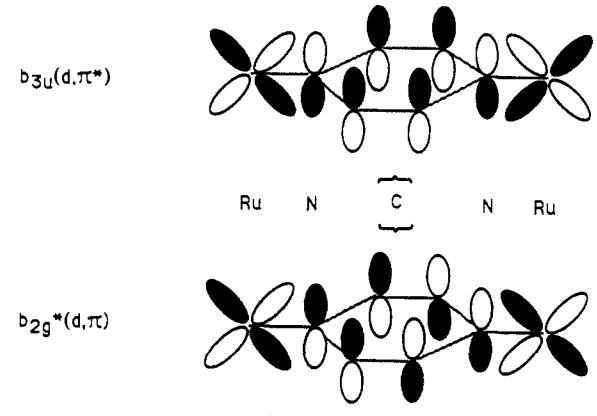

Figure 3. Sketches of the $b_{3u}(d,\pi^*)$ and $b_{2g}^*(d,\pi)$ molecular orbitals.

π^* orbital of b_{3u} symmetry, but on energetic grounds the most important interactions are expected to be with the pyrazine $b_{3u}(\pi^*)$ LUMO and with the pyrazine $b_{2g}(\pi)$ MO to give mixed-valence orbitals of the form (c_1, c_2, d_1, and $d_2 > 0$)

$$|b_{3u}(\mathrm{d},\pi^*)\rangle = (c_1/\sqrt{2})(|b_2(\mathrm{A})\rangle - |b_2(\mathrm{B})\rangle) + c_2|b_{3u}(\pi^*)\rangle$$
$$|b_{2g}^*(\mathrm{d},\pi)\rangle = (d_1/\sqrt{2})(|b_2(\mathrm{A})\rangle + |b_2(\mathrm{B})\rangle) - d_2|b_{2g}(\pi)\rangle \qquad (4)$$

and, of course, their $b_{3u}^*(\pi^*,\mathrm{d})$ and $b_{2g}(\pi,\mathrm{d})$ analogues. The $b_{3u}(\mathrm{d},\pi^*)$ and $b_{2g}^*(\mathrm{d},\pi)$ MO's are sketched in Figure 3.

As illustrated in Figure 2, the lowest energy excitations should involve the orbitals of eqs 3 and 4. Thus, our electronic basis states are

$$\varphi_1 = |^2B_{2g} \pm \tfrac{1}{2}\rangle = |b_{3u}^2a_g^2b_{1u}^2b_{3g}^2b_{2u}^2b_{2g}^{*\pm}\rangle$$
$$\varphi_2 = |^2A_g \mp \tfrac{1}{2}\rangle = |b_{3u}^2a_g^{\mp}b_{1u}^2b_{3g}^2b_{2u}^2b_{2g}^{*2}\rangle$$
$$\varphi_3 = |^2B_{1u} \mp \tfrac{1}{2}\rangle = |b_{3u}^2a_g^2b_{1u}^{\mp}b_{3g}^2b_{2u}^2b_{2g}^{*2}\rangle$$
$$\varphi_4 = |^2B_{3g} \pm \tfrac{1}{2}\rangle = -|b_{3u}^2a_g^2b_{1u}^2b_{3g}^{\pm}b_{2u}^2b_{2g}^{*2}\rangle$$
$$\varphi_5 = |^2B_{2u} \pm \tfrac{1}{2}\rangle = -|b_{3u}^2a_g^2b_{1u}^2b_{3g}^2b_{2u}^{\pm}b_{2g}^{*2}\rangle$$
$$\varphi_6 = |^2B_{3u} \pm \tfrac{1}{2}\rangle = |b_{3u}^{\pm}a_g^2b_{1u}^2b_{3g}^2b_{2u}^2b_{2g}^{*2}\rangle \qquad (5)$$

The kets designate Slater determinants, and the negative signs

ensure that the kets obey the hole-particle convention.[6] If the Ru centers were truly octahedral and there were no electronic, spin–orbit, or vibronic coupling perturbations, the states of eq 5 would be degenerate.

Electronic Coupling Perturbation. The interaction between the Ru centers and the pyrazine bridge splits the degeneracy of the eq 5 basis states. The most important interactions are those depicted in the Figure 2 MO diagram.[7] They leave $|^2B_{2g} \pm {}^1/_2\rangle$ as the ground state. Next in energy come the $|^2A_g \mp {}^1/_2\rangle$, $|^2B_{1u} \mp {}^1/_2\rangle$ pair followed by the $|^2B_{3g} \pm {}^1/_2\rangle$, $|^2B_{2u} \pm {}^1/_2\rangle$ pair. Finally, $|^2B_{3u} \pm {}^1/_2\rangle$ lies highest. Spin–orbit coupling mixes states of like parity and splits the degeneracies of the pairs. The C–T ion mixed-valence band arises essentially from the strongly allowed, z-polarized $b_{3u}(d,\pi^*) \rightarrow b_{2g}^*(d,\pi)$ excitation[7,4] or, equivalently, from the $|^2B_{2g} \pm {}^1/_2\rangle \rightarrow |^2B_{3u} \pm {}^1/_2\rangle$ transition. It is the only low-energy transition allowed in the one-center approximation in the absence of spin–orbit coupling and higher order effects.

The major electronic perturbation is the interaction of Ru symmetry orbitals with π and π^* orbitals of the pyrazine bridge. This is supported by X-ray data[8] for the Creutz–Taube ion, $[Ru(NH_3)_5]_2pyz^{5+}$ (the II,III complex), for $[Ru(NH_3)_5]_2pyz^{4+}$ (the II,II complex), and for $[Ru(NH_3)_5]_2pyz^{6+}$ (the III,III complex). Bond lengths of II,III and II,II show clear evidence of π^* back-bonding between Ru and the pyrazine ring, while III,III shows no signs of back-donation.[8] Compared with the III,III complex, II,III has a shorter Ru–N(pyr) bond (by 0.124 Å), a longer pyrazine C–N bond (by 0.021 Å), a shorter pyrazine C–C bond (by 0.021 Å), a longer Ru–N(trans) bond (by 0.034 Å), and a longer Ru–N(cis) bond (by 0.011 Å). C–N and C–C bond lengths of III,III are close to those in free pyrazine. In the II,III complex, Ru–N(pyr), Ru–N(trans), and Ru–N(cis) bond lengths average 1.991, 2.123, and 2.112 Å, while in III,III they average 2.115, 2.089, and 2.101 Å, respectively.

The large decrease in the Ru–N(pyr) bond length and the accompanying smaller changes in the pyrazine C–C and C–N bond lengths are generally cited as clear evidence of back-bonding between Ru and the pyrazine ring.[8] In the II,III and II,II complexes (but *not* in the III,III complex), considerable electron density is transferred from the $b_{3u}(d)$ Ru symmetry orbital to the $b_{3u}(\pi^*)$ pyrazine orbital upon formation of the $b_{3u}(d,\pi^*)$ MO. As is clear from the $b_{3u}(d,\pi^*)$ MO sketch in Figure 3, this transfer contributes to the bond length changes.

Recent data on the lack of solvent dependence of the $b_{3u}(d,\pi^*) \rightarrow b_{2g}^*(d,\pi)$ (mixed-valence) and $b_{2g}^*(d,\pi) \rightarrow b_{3u}^*(\pi^*,d)$ ($d \rightarrow \pi^*$) bands of $[Ru(NH_3)_5]_2pyz^{5+}$ as compared to solvent dependence data for related compounds have led Creutz and Chou[9] to conclude that considerable π bonding between Ru and pyrazine also occurs. This is the interaction that leads to formation of the $b_{2g}(\pi,d)$ and $b_{2g}^*(d,\pi)$ MO's in Figure 2. They suggest the interaction is sufficiently strong to give our Figure 2 parameters, $\epsilon(b_{2g}^*)$ and $\epsilon(b_{3u})$, roughly equal magnitudes of 3000 cm^{-1}. The $b_{2g}^*(d,\pi)$ MO is sketched in Figure 3.

In the ground configuration, the bonding $b_{2g}(\pi,d)$ MO is doubly occupied while the antibonding $b_{2g}^*(d,\pi)$ MO contains a single electron. Thus, the net result of this π bonding is the removal of electron density from the $b_{2g}(\pi)$ pyrazine orbital and the buildup Ru–N(pyr) electron density. This augments the bond length changes induced by π^* back-bonding.

Fits of the Creutz–Taube ESR data require a substantial shift of the $|^2B_{2g} \pm {}^1/_2\rangle$ state downward in energy relative to the $|^2A_g \mp {}^1/_2\rangle$ and $|^2B_{3g} \pm {}^1/_2\rangle$ states of eq 5. The most logical source of this shift is once again π bonding between $b_{2g}(d)$ and $b_{2g}(\pi)$ discussed above, which shifts the $b_{2g}^*(d,\pi)$ MO upward by $\epsilon(b_{2g}^*)$ relative to the $\gamma(d)$ MO's (see Figure 2). Thus, the experimental evidence suggests that both π^* back-bonding and π bonding are significant.

The $\epsilon(b_{2g}^*)$ and $-\epsilon(b_{3u})$ energy shifts illustrated in Figure 2 are the MO explanation of the "rhombic splitting" of the Ru t_{2g} orbitals in the crystal field picture. Note that the shifts are in *opposite* directions for the $b_{2g}(d)$ and $b_{3u}(d)$ symmetry orbitals. The $a_g(d)$, $b_{1u}(d)$, $b_{3g}(d)$, and $b_{2u}(d)$ symmetry orbitals are orthogonal to the pyrazine π system and are unaffected by it. In fact, there are no apparent significant interactions between these orbitals and the orbitals of the pyrazine bridge.

Reasonable fits of the ESR data also require that the $|^2A_g \mp {}^1/_2\rangle$ state be shifted downward somewhat as compared to the $|^2B_{3g} \pm {}^1/_2\rangle$ state. This shift is related to the splittings of the pseudo-t_{2g} orbitals. As discussed above, the $a_g(d)$, $b_{1u}(d)$, $b_{3g}(d)$, and $b_{2u}(d)$ orbitals do not participate in MO formation with the pyrazine bridge. However the energies of all the pseudo-t_{2g} orbitals are affected by the different potential of the pyrazine N as compared to the ammonia N's. As documented above, the Ru–N(pyr) bond is noticeably shorter than the cis and trans Ru–N(ammonia) bonds in the Creutz–Taube complex, II,III. This leads to a small tetragonal distortion that shifts the $a_g(d)$ and $b_{1u}(d)$ orbital energies by $\epsilon(tet)$ relative to the energies of $b_{3g}(d)$, $b_{2u}(d)$, $b_{2g}(d)$, and $b_{3u}(d)$ orbitals (see Figure 2). We take our zero of energy in Figure 2 as the $b_{3g}(d)$, $b_{2u}(d)$ orbital energy.

All our eq 5 basis states arise from single-hole configurations. Thus, in the absence of other perturbations, the relative energy of each state is simply the negative of its hole-MO energy. It follows that the relative energies of our basis states in the order they are listed in eq 5 are $-\epsilon(b_{2g}^*)$, $-\epsilon(tet)$, $-\epsilon(tet)$, 0, 0, and $\epsilon(b_{3u})$.

Estimation of Electronic Perturbation Parameters. To treat electronic coupling, we must estimate the parameters in Figure 2. We do this as much as possible from spectroscopic data. We use the electronic spectrum of the Creutz–Taube ion[2b] along with the considerations discussed above. Our method is similar to that of ref 9. In the absence of spin–orbit coupling, each allowed excitation of interest gives rise to only one allowed transition. The spectroscopic transition energies may be expressed in terms of the Figure 2 parameters. Thus, the mixed-valence band with a maximum at approximately 6400 cm^{-1} lets us estimate $\Delta = \epsilon(b_{3u}) + \epsilon(b_{2g}^*)$ to be around 6400 cm^{-1} (as the spin–orbit coupling parameter ζ is increased, this sum must be reduced somewhat to fit the energy maximum of the mixed-valence band). Similarly, the $b_{2g}^*(d,\pi) \rightarrow b_{3u}^*(\pi^*,d)$ band with a maximum at 17 700 cm^{-1} gives $\alpha(\pi_u^*) + \epsilon(b_{3u}) - \epsilon(b_{2g}^*) \approx 17\,700$ cm^{-1}. Finally the band at around 40 000 cm^{-1} is assigned to a transition arising from the $b_{2g}(\pi,d) \rightarrow b_{3u}^*(\pi^*,d)$ excitation. This gives $\alpha(\pi_g) + \alpha(\pi_u^*) + \epsilon(b_{3u}) + \epsilon(b_{2g}^*) \approx 40\,000$ cm^{-1}.

These are the only *allowed* one-electron excitations among the Figure 2 MO's. However, the *forbidden* $b_{1u}(d) \rightarrow b_{2g}^*(d,\pi)$ and $b_{2u}(d) \rightarrow b_{2g}^*(d,\pi)$ excitations should give rise to bands in the infrared that become allowed due to spin–orbit coupling. In the absence of spin–orbit coupling these excitations have energies of $\epsilon(b_{2g}^*) - \epsilon(tet)$ and $\epsilon(b_{2g}^*)$, respectively. However, of the low-energy electronic transitions, only the mixed-valence band is well-resolved. There is some indication from MCD results[10] of weak electronic bands in the 2000–2700- and 3200–3600-cm^{-1} regions. The 3200–3600-cm^{-1} band appears to be vibronically induced and so may arise from a *parity*-forbidden excitation.

The spectroscopic data for the *allowed* transitions give us three equations with four unknowns: $\alpha(\pi_g)$, $\alpha(\pi_u^*)$, $\epsilon(b_{3u})$, $\epsilon(b_{2g}^*)$. Rough estimates of one of these unknowns, $\epsilon(b_{2g}^*)$, and of $\epsilon(tet)$ can then be made from the weak MCD bands observed below 4000 cm^{-1}, and ESR data can further be used to narrow parameter choices. We find that when $\lambda^{PKS} = 1.1$ (see discussion of off-diagonal vibronic constants ahead), an acceptable fit of the experimental g values requires that we choose $\epsilon(b_{2g}^*)/\zeta$ in the range 2.6-3.0 and $\epsilon(tet)/\zeta$ in the range 0.75-0.77. Thus, if all the available experimental data are used collectively, our electronic parameters are fairly well-defined.

Once we have estimated $\alpha(\pi_u^*)$, $\alpha(\pi_g)$, $\epsilon(b_{3u})$, and $\epsilon(b_{2g}^*)$, we can work backward to obtain the electronic coupling parameters

(6) Piepho, S. B.; Schatz, P. N. *Group Theory in Spectroscopy*; Wiley-Interscience: New York, 1983.
(7) Lauher, J. W. *Inorg. Chim. Acta* **1980**, *39*, 119–123.
(8) Fürholz, U.; Joss, S.; Bürgi, H. B.; Ludi, A. *Inorg. Chem.* **1985**, *24*, 943–948.
(9) Creutz, C.; Chou, M. H. *Inorg. Chem.* **1987**, *26*, 2995–3000.
(10) (a) Krausz, E. *Chem. Phys. Lett.* **1985**, *120*, 113–117. (b) Krausz, E.; Mau, A. W. H. *Inorg. Chem.* **1986**, *25*, 1484–1488.

$J(b_{3u}) = \langle b_{3u}(\pi^*)|h^{elec}|b_{3u}(d)\rangle$ and $J(b_{2g}) = \langle b_{2g}(\pi)|h^{elec}|b_{2g}(d)\rangle$ and hence the 2×2 b_{3u} and b_{2g} orbital energy matrices. The MO mixing coefficients c_1, c_2, d_1, and d_2 in eq 4 can then be determined. Thus, $J(b_{3u})$, $J(b_{2g})$, and the MO coefficients are quantities calculated from our electronic parameters (see Table II for examples).

Spin–Orbit Coupling Perturbation. Spin–orbit coupling mixes basis states of eq 5 that have the same parity. As a result of this mixing, transitions from the ground state to the (nominal) $|^2B_{1u} \mp {}^1/_2\rangle$ and $|^2B_{2u} \pm {}^1/_2\rangle$ states become weakly allowed in the z polarization.

The $\mathbf{H}_{so}$ matrix elements are calculated by first reducing them to one-electron form. The MO's are then expanded in terms of Ru AO's and pyrazine π or π^* functions with eqs 2 and 4. All two-center terms are dropped, and since the ζ_{2p} for N and C are negligible compared to ζ_{4d} for Ru, the single-center pyrazine contributions are also neglected. The remaining integrals are expressed in terms of Ru 4d functions by eq 1 and are easily evaluated by standard methods.

Vibrational Basis. Strong vibronic interactions involve vibrational coordinates that change significantly during adiabatic electron transfer. The C–T complex is a *delocalized* mixed-valence system, and the mixed-valence transition arises primarily from the $b_{3u}(d,\pi^*) \rightarrow b_{2g}{}^*(d,\pi)$ excitation as discussed above. Thus, the totally symmetric coordinate that connects the bond lengths before and after the $b_{3u}(d,\pi^*) \rightarrow b_{2g}{}^*(d,\pi)$ excitation is expected to play the primary role in determining the shape of the C–T mixed-valence band.[1] We term this coordinate Q_+^{mol} (mol = molecular).

If the C–T complex were a highly *localized* mixed-valence complex, stable states of the ions would have either Ru(A) oxidized to Ru(III) and Ru(B) reduced to Ru(II) or vice versa. In that case the totally symmetric coordinates of A and B (Q_A and Q_B), which change the shorter equilibrium bond lengths of Ru(II) to those of Ru(III) and vice versa, would be strongly coupled vibronically. We include these coordinates in our vibrational basis in symmetry-adapted form.

Thus, our vibrational basis consists of Q_+^{mol} and the symmetry-adapted linear combinations of the single-center (localized = loc) coordinates Q_A and Q_B:

$$Q_1(A_g) = Q_+^{mol}$$

$$Q_2(B_{1u}) = Q_-^{loc} = (1/\sqrt{2})(Q_A - Q_B)$$

$$Q_3(A_g) = Q_+^{loc} = (1/\sqrt{2})(Q_A + Q_B) \qquad (6)$$

Vibronic Coupling Perturbation. The vibronic coupling perturbation adds terms to the Hamiltonian of the type

$$l_\alpha^{(j)} Q_\alpha = (\sqrt{2}h\nu_\alpha)\lambda_\alpha^{(j)} q_\alpha$$

$$l_\alpha^{(jj')} Q_\alpha = (\sqrt{2}h\nu_\alpha)\lambda_\alpha^{(jj')} q_\alpha \qquad (7)$$

where the right-hand side uses dimensionless coordinates.[1] The l and the λ are linear vibronic coupling constants that parameterize the perturbation. They are defined as

$$l_\alpha^{(j)} = \langle \varphi_j^{(0)}|(\partial V/\partial Q_\alpha)_{Q_0}|\varphi_j^{(0)}\rangle$$

$$l_\alpha^{(jj')} = \langle \varphi_j^{(0)}|(\partial V/\partial Q_\alpha)_{Q_0}|\varphi_{j'}^{(0)}\rangle \qquad (8)$$

The $\varphi_j^{(0)}$ are zero-order electronic solutions to the electronic Hamiltonian at the ground-state nuclear configuration $Q_0 = 0$. Since the ground-state nuclear coordinates are chosen so that $Q_0 = 0$ at the potential minima, $(\partial V/\partial Q_\alpha)_{Q_0} = 0$ for all α of the ground state. Thus

$$l_\alpha^{(1)} = 0 \text{ (for all } \alpha) \qquad (9)$$

(and hence $\lambda_\alpha^{(1)} = 0$ for all α).

Diagonal Vibronic Constants. We first express our vibronic coupling constants in terms of orbital vibronic constants (OVC's), $\langle\gamma|(\partial v(i)/\partial Q_\alpha)_{Q_0}|\gamma'\rangle$, where γ and γ' are molecular orbitals. Since $(\partial V/\partial Q_\alpha)_{Q_0}$ is a one-electron operator and the $l_\alpha^{(1)}$ are zero for all α, it is easy to show[1] that for $\alpha = 1$ and 3 and $j = 2$–6

$$l_\alpha^{(j)} = \langle \varphi_j^{(0)}|(\partial V/\partial Q_\alpha)_{Q_0}|\varphi_j^{(0)}\rangle = -\langle\gamma|(\partial v(i)/\partial Q_\alpha)_{Q_0}|\gamma\rangle + \langle b_{2g}{}^*|(\partial v(i)/\partial Q_\alpha)_{Q_0}|b_{2g}{}^*\rangle \qquad (10)$$

where γ is the hole orbital in the respective eq 5 function. The $l_2^{(j)}$ are zero by symmetry; diagonal vibronic constants for nondegenerate MO's are nonzero only for totally symmetric vibrational modes.

The magnitude of a diagonal OVC for a given orbital and totally symmetric vibration Q_α is related to the sensitivity of the electron distribution in the MO to motion along the coordinate Q_α. Bersuker[5] argues that the value of a diagonal OVC for a given MO and a given totally symmetric vibrational mode ν_α is equal to the force with which an electron in the MO distorts the nuclear framework in the direction of the totally symmetric displacement Q_α minus the proportion of the internuclear repulsion in this direction per electron. Contributions to a diagonal OVC for a vibrational coordinate that stretches a bond A–B are most often positive for an MO bonding with respect to the A–B bond, negative for an MO antibonding with respect to the A–B bond, and ca. zero for MO's nonbonding with respect to the A–B bond.

Let us first consider the OVC's for $Q_1(A_g)$, the totally symmetric coordinate that connects the bond lengths before and after the $b_{3u}(d,\pi^*) \rightarrow b_{2g}{}^*(d,\pi)$ excitation. The diagonal OVC's for Q_1 should be negligible for $\gamma = a_g$, b_{1u}, b_{3g}, and b_{2u} since these MO's are linear combinations of Ru 4d orbitals that are perpendicular to the xz plane and do not participate in σ or π bonding with pyrazine (see eqs 1 and 3 and Figure 1). They are nonbonding along the bonds affected by the Q_1 stretching motion. On the other hand, the Q_1 OVC's should be significant for the $b_{2g}{}^*$ and b_{3u} MO's of eq 4, which are sketched in Figure 3. We expect the $b_{2g}{}^*(d,\pi)$ OVC for Q_1 to be opposite in sign to the $b_{3u}(d,\pi^*)$ OVC since the $b_{2g}{}^*(d,\pi)$ MO is bonding where the $b_{3u}(d,\pi^*)$ MO is antibonding and it is antibonding where the $b_{3u}(d,\pi^*)$ MO is bonding. Thus, for $l_1^{(6)}$, the $b_{2g}{}^*$ and b_{3u} OVC are additive in eq 10. However, since both the $b_{2g}{}^*$ and b_{3u} OVC include both bonding and antibonding contributions, some cancellation is expected so the magnitudes of these OVC should be small. If we write

$$\langle b_{3u}|(\partial v(i)/\partial Q_1)_{Q_0}|b_{3u}\rangle = -\kappa\langle b_{2g}{}^*|(\partial v(i)/\partial Q_1)_{Q_0}|b_{2g}{}^*\rangle \qquad (11)$$

(where κ is estimated to be ≈ 1), it follows that, for the $Q_1(A_g)$ OVC's of eq 10, we have

$$l_1^{(2)} = l_1^{(3)} = l_1^{(4)} = l_1^{(5)} = (1+\kappa)^{-1} l_1^{(6)} \qquad (12)$$

and hence

$$\lambda_1^{(2)} = \lambda_1^{(3)} = \lambda_1^{(4)} = \lambda_1^{(5)} = (1+\kappa)^{-1}\lambda_1^{(6)} \qquad (13)$$

Next we consider the diagonal OVC of eq 10 for $Q_3(A_g) = (1/\sqrt{2})(Q_A + Q_B)$. Since Q_A and Q_B are symmetric stretching modes on the Ru(A) and Ru(B) centers, diagonal OVC's for $Q_3(A_g)$ should be negligible for orbitals that are nonbonding with respect to the Ru–N bonds. This is the case for all our eq 3 orbitals, while our eq 4 MO's involve Ru–N(pyr) π bonding. We implicitly assume, however, that in our vibrational basis the Ru–N(pyr) stretch predominates in Q_1 and is a minor component in Q_2 and Q_3. Thus, we conclude that $l_3^{(j)} \approx 0$ for $j = 2$–6. In the next section we arrive at a similar conclusion using another approach.

Off-Diagonal Vibronic Constants. Nonzero off-diagonal vibronic coupling constants involve $Q_2 = (1/\sqrt{2})(Q_A - Q_B)$ of eq 6, which is the Q_- mode of the PKS model. They govern the magnitude of the pseudo-Jahn–Teller (PJT) effect and are easily related to the PKS vibronic coupling parameter,[3] l^{PKS} (and hence to its dimensionless equivalent λ^{PKS}). The method is based on the assumption that Q_A and Q_B are localized modes on centers A and B. Thus, the Q_2 (and Q_3) OVC can be expressed in terms of Q_A and Q_B OVC localized on centers A and B, respectively. These are the l^{PKS} OVC of the PKS model (see eq 41 of ref 1). The procedure is outlined in ref 1.

Table I. Electronic Potential Energy Matrix[a]

	φ_1	φ_2	φ_3	φ_4	φ_5	φ_6
φ_1	$-\epsilon(b_{2g}^*) + \Omega_0$	$(d_1/2)\theta\zeta$	0	$(d_1/2)\theta\zeta$	0	$-c_1d_1h\nu_2\lambda^{PKS}q_2$
φ_2	$(d_1/2)\theta\zeta$	$-\epsilon(\text{tet}) + \Omega$	$-h\nu_2\lambda^{PKS}q_2$	$-\zeta/2$	0	0
φ_3	0	$-h\nu_2\lambda^{PKS}q_2$	$-\epsilon(\text{tet})+\Omega$	0	$-\zeta/2$	$(c_1/2)\theta\zeta$
φ_4	$(d_1/2)\theta\zeta$	$-\zeta/2$	0	Ω	$-h\nu_2\lambda^{PKS}q_2$	0
φ_5	0	0	$-\zeta/2$	$-h\nu_2\lambda^{PKS}q_2$	Ω	$(c_1/2)\theta\zeta$
φ_6	$-c_1d_1h\nu_2\lambda^{PKS}q_2$	0	$(c_1/2)\theta\zeta$	0	$(c_1/2)\theta\zeta$	$\epsilon(b_{3u}) + \Omega'$

[a] The electronic basis is that of eq 5. The dimensionless vibronic coordinates of eq 7 are used. $\theta = \pm 1$ for the upper and lower spins, respectively, in the eq 5 basis. $\Omega_0 = {}^1/_2\sum_{\alpha=1\text{-}3}h\nu_\alpha q_\alpha^2$. $\Omega = [\sqrt{2}/(1+\kappa)]h\nu_1\lambda_1^{(6)}q_1 + (1-c_1^2)h\nu_3\lambda^{PKS}q_3 + \Omega_0$. $\Omega' = [\sqrt{2}h\nu_1\lambda_1^{(6)}q_1 + (d_1^2 - c_1^2)h\nu_3\lambda^{PKS}q_3 + \Omega_0$.

Nonzero off-diagonal vibronic coupling constants, expressed first in terms of OVC's and then in terms of l^{PKS}, are

$$\begin{aligned} l_2^{(1,6)} = l_2^{(6,1)} &= \langle\varphi_1^{(0)}|(\partial V/\partial Q_2)_{Q_0}|\varphi_6^{(0)}\rangle \\ &= -\langle b_{3u}|(\partial v(i)/\partial Q_2)_{Q_0}|b_{2g}^*\rangle \\ &= -c_1d_1(1/\sqrt{2})l^{PKS} \\ l_2^{(2,3)} = l_2^{(3,2)} &= \langle\varphi_2^{(0)}|(\partial V/\partial Q_2)_{Q_0}|\varphi_3^{(0)}\rangle \\ &= -\langle b_{1u}|(\partial v(i)/\partial Q_2)_{Q_0}|a_g\rangle \\ &= -(1/\sqrt{2})l^{PKS} \\ l_2^{(4,5)} = l_2^{(5,4)} &= \langle\varphi_4^{(0)}|(\partial V/\partial Q_2)_{Q_0}|\varphi_5^{(0)}\rangle \\ &= -\langle b_{2u}|(\partial v(i)/\partial Q_2)_{Q_0}|b_{3g}\rangle \\ &= -(1/\sqrt{2})l^{PKS} \end{aligned} \quad (14)$$

Note that $l_2^{(1,6)}$ is diminished in value relative to $l_2^{(2,3)}$ and $l_2^{(4,5)}$ because of MO formation; since Q_A and Q_B are metal-center stretching modes, the bridge-orbital parts of the $b_{3u}(d,\pi^*)$ and the $b_{2g}^*(d,\pi)$ MO's (see eq 4) make no contribution to the OVC. Equation 14 also can be used to relate the $\lambda_2^{(i,j)}$ to λ^{PKS} by replacing the l's with λ's.

The PKS model[3] predicts that l^{PKS} (and hence λ^{PKS}) will be proportional to the difference in bond lengths between the oxidized and reduced forms of the metal ion centers. This idea helps us estimate the magnitude of the off-diagonal vibronic coupling constants. In the case of the Creutz–Taube ion, the difference in bond lengths between the oxidized and reduced forms of the metal ion centers is 0.04 Å, and it follows that $\lambda^{PKS} = 1.1$.[11] We use this value in our calculations. When λ^{PKS} has this magnitude, vibronic coupling to $Q_2 = (1/\sqrt{2})(Q_A - Q_B)$ of eq 6 (which is the Q_- mode of the PKS model) has very little effect on the C–T band shape.

One can use the same procedure as above to estimate the values of the diagonal OVC for $Q_3 = (1/\sqrt{2})(Q_A + Q_B)$ of eq 6 (which is the Q_+ mode of the PKS model) with the results

$$\begin{aligned} l_3^{(2)} = l_3^{(3)} = l_3^{(4)} = l_3^{(5)} &= (d_1^2 - 1)(1/\sqrt{2})l^{PKS} \\ l_3^{(6)} &= (d_1^2 - c_1^2)(1/\sqrt{2})l^{PKS} \end{aligned} \quad (15)$$

Since c_1 and d_1, the MO coefficients of eq 4, are ≥ 0.9 (see Table II), the l_3 OVC are very small. In fact, when we do a three-mode calculation with $\lambda^{PKS} = 1.1$, the results are essentially identical with those of the two-mode calculation in which coupling to Q_3 is neglected. This result was anticipated by our remarks above in the section on diagonal OVC.

High-Pressure Studies. Recently Hammack et al.[12] have studied the effect of pressure on the energy and band shape of the mixed-valence band of the C–T ion in various media. They find that the band energy increases as the pressure increases. However, except for variations in the position of a weak shoulder (see discussion below), the band shape changes relatively little. As pointed out by the authors, the band energy increase is consistent with the mixed-valence band being essentially a bonding → antibonding transition. As the pressure increases, electronic coupling increases so the band energy increases.

The absence of large changes in the band shape with pressure probably results from the cancellation of two opposing effects. The discussion of diagonal OVC above suggests that the $\lambda_1^{(j)}$ for $j = 2$–6 should increase, and hence the band should broaden, as the pressure increases. This follows since increases in pressure augment the bonding/antibonding interactions. On the other hand, eq 14 shows that $l_2^{(1,6)}$ (and hence $\lambda_2^{(1,6)}$) decreases as electronic coupling increases because c_1 and d_1 diminish (see eq 4) as π^* and π interactions increase; this leads to a decrease in bandwidth with increasing pressure. In addition, since $\lambda_2^{(1,6)}$ acts off-diagonal, its effect is diminished as the electronic coupling increases with increasing pressure; again this narrows the bandwidth as pressure increases. If the above (opposing) tendencies cancel, the band shape would change little with pressure as observed.

Electronic Potential Energy Matrix. The electronic potential energy matrix including the effects of electronic, spin–orbit, and vibronic coupling to Q_1, Q_2, and Q_3 is given in Table I. As discussed above, Q_3 should play a negligible role in the vibronic coupling.

Solution of the Dynamic Problem. Nuclear kinetic energy terms are added to the Table I matrix to give the dynamic matrix for the problem. The dynamic matrix is then diagonalized in a harmonic oscillator basis to obtain eigenvalues and eigenvectors.[1] We *do not* make the Born–Oppenheimer approximation, and when the off-diagonal vibronic coupling constants are nonzero, the electronic basis states are coupled vibronically. Then nuclear motion is not confined to a single surface, and the Born–Oppenheimer approximation breaks down.

Eigenvalues and eigenvectors may be determined to arbitrary accuracy by choosing the vibronic basis sufficiently large.[1] These are then used to calculate the absorption profile and the g values for the mixed-valence complex. If we have six electronic states in our basis (as in eq 5), include two vibrational modes (Q_1 and Q_2), and limit the total number of excited vibrational quanta to n, the dimension of the dynamic matrix is $6(n+1)(n+2)/2$.[1]

Calculation of the Absorption Profile. To obtain the absorption profile, the dipole strength is calculated for each vibronic line. The method is described in detail in ref 1. For the calculation we need to provide electric dipole matrix elements between the electronic states of eq 5. These may be calculated with either the dipole length or dipole velocity expressions. The two methods should give the same results for spin-allowed transitions *if exact wave functions are employed.* In practice, *approximate* wave functions are always used and quite different results are typically obtained by the two methods. Studies of atomic transitions for which the optical intensities are accurately known show that in some cases the dipole length expression and in other cases the dipole velocity expression gives results closer to experiment.[13] More elaborate methods have been proposed that may be used in some cases to improve upon results obtained by one or the other of these forms.[14] For molecular transitions there is some indication that dipole velocity intensities are more accurate than dipole length intensities for delocalized π-electron systems.[15] The dipole velocity formalism is commonly used to calculate circular dichroism (CD) intensities to ensure origin independence of the calculated CD.[16]

(11) Wong, K. Y.; Schatz, P. N. *Prog. Inorg. Chem.* **1981**, *28*, 369–449.
(12) Hammack, W. S.; Lowery, M. D.; Hendrickson, D. N.; Drickamer, H. G. *J. Phys. Chem.* **1988**, *92*, 1771–1774.
(13) (a) Crossley, R. J. S. *Adv. At. Mol. Phys.* **1969**, *5*, 237–296. (b) Anderson, M. T.; Weinhold, F. *Phys. Rev. A* **1974**, *10*, 1457–1463.
(14) (a) Roginsky, D. V. I.; Klapisch, M.; Cohen, M. *Chem. Phys. Lett.* **1983**, *95*, 568–572. (b) Laughlin, C. *Chem. Phys. Lett.* **1984**, *106*, 170–174.
(15) McHugh, A. J.; Gouterman, M. *Theor. Chim. Acta (Berlin)* **1969**, *13*, 249–258.

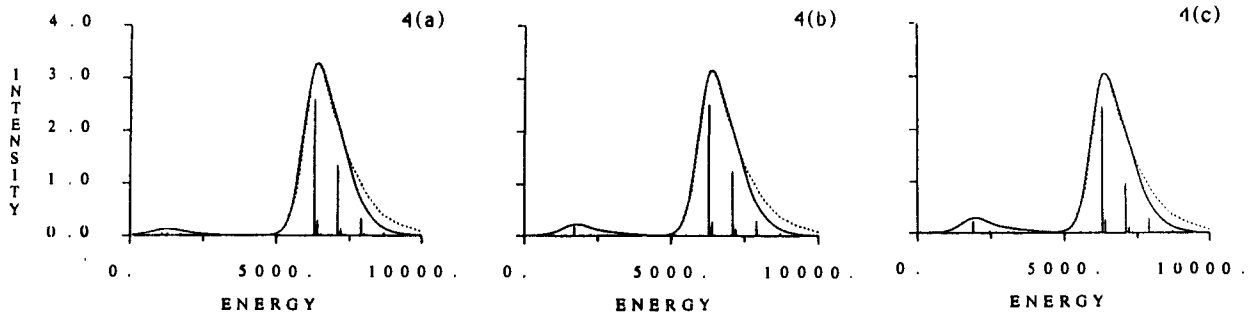

Figure 4. Two-mode calculated absorption profile at 298 K with $\lambda_1^{(6)} = 0.7$ and $\nu_1 = 800$ cm^{-1}. For further details, see Table II and section III of the text. The dashed curve is the experimental absorption spectrum from ref 2a.

In our case the mixed-valence band is z-polarized. In the absence of spin–orbit coupling, all the intensity comes from $\varphi_1^0 = |^2B_{2g} \pm {}^1/_2\rangle \rightarrow \varphi_6^0 = |^2B_{3u} \pm {}^1/_2\rangle$ contributions. Spin–orbit coupling mixes basis states of eq 5 that have the same parity. However, in the dipole velocity case no new source of intensity develops when spin–orbit coupling is included since the $\varphi_2^0 = |^2A_g \mp {}^1/_2\rangle \rightarrow \varphi_3^0 = |^2B_{1u} \mp {}^1/_2\rangle$ and $\varphi_4^0 = |^2B_{3g} \pm {}^1/_2\rangle \rightarrow \varphi_5^0 = |^2B_{2u} \pm {}^1/_2\rangle$ transitions, which are formally allowed, have negligible intensity. These are d → d transitions in our basis, and the one-center dipole velocity terms are zero by parity, while the two-center terms are negligible since they involve d orbitals on two widely separated Ru atoms. Likewise, in the dipole velocity case one-center terms do not contribute to the intensity of the $\varphi_1^0 = |^1B_{2g} \pm {}^1/_2\rangle \rightarrow \varphi_6^0 = |^2B_{3u} \pm {}^1/_2\rangle$ transition; however, for this transition the two-center terms are significant since some of the contributing atomic centers are closer together as a result of the π bonding in the $b_{2g}^*(d,\pi)$ and $b_{3u}(d,\pi^*)$ MO's.

In the dipole length case, the mixed-valence intensity comes largely from one-center d → d contributions that are nonzero upon transformation of the dipole length operator to the Ru centers. In the absence of π bonding in the $b_{2g}^*(d,\pi)$ and $b_{3u}(d,\pi^*)$ MO's, the $\varphi_2^0 = |^2A_g \mp {}^1/_2\rangle \rightarrow \varphi_3^0 = |^2B_{1u} \mp {}^1/_2\rangle$, $\varphi_4^0 = |^2B_{3g} \pm {}^1/_2\rangle \rightarrow \varphi_5^0 = |^2B_{2u} \pm {}^1/_2\rangle$, and $\varphi_1^0 = |^2B_{2g} \pm {}^1/_2\rangle \rightarrow \varphi_6^0 = |^2B_{3u} \pm {}^1/_2\rangle$ transitions all have a z-polarized transition moment of magnitude 3.408 e Å (e = electronic charge; 3.408 Å = distance between a Ru atom and the molecular origin[8]). In the dipole length formalism the intensity of the $\varphi_1^0 \rightarrow \varphi_6^0$ transition is *diminished* somewhat by π bonding. In contrast, recall in the dipole velocity formalism that the intensity of the same transition is *nonzero* as a *result* of the π bonding, and the other transitions are essentially forbidden!

Given the very different mechanisms governing intensity in the dipole length and dipole velocity formalisms, it is not surprising that the methods give different absolute intensities for the C–T absorption profile. As pointed out some years ago, the dipole length approximation overestimates the intensity of the mixed-valence band by a considerable margin.[17] We find that the dipole velocity approximation also overestimates it, but by a much smaller margin. Using the conventions of Appendix A.6 of ref 6 and the experimental oscillator strength of the C–T mixed-valence band, $f = 0.03$,[2b] we calculate an experimental dipole strength for the band of 3.3 D^2 (D = debye; 4.803 D = 1 e Å). In comparison, theoretical values with Slater orbitals and our Figure 4 parameters are approximately 11 D^2 by the dipole velocity formalism and 50 D^2 by the dipole length formalism. Clearly, the dipole velocity formalism gives a more realistic magnitude here.

The two formalisms predict nearly the same band shape for the mixed-valence band, although the dipole length expression reproduces the experimental high-energy tail of the band slightly better (as we discuss ahead, this is probably not significant since experimental evidence suggests this tail is due to non totally symmetric vibronic structure not included in our model). However, quite different dispersions and absolute intensities are calculated for the bands below 5000 cm^{-1} by the two methods. In our model these bands arise from (a) infrared transitions between low-lying vibronic levels of opposite parity that gain intensity through vibronic coupling to $Q_2 = Q_-^{loc}$ and (b) from the orbitally forbidden $\varphi_1^0 = |^2B_{2g} \pm {}^1/_2\rangle \rightarrow \varphi_3^0 = |^2B_{1u} \mp {}^1/_2\rangle$ and $\varphi_1^0 = |^2B_{2g} \pm {}^1/_2\rangle \rightarrow \varphi_5^0 = |^2B_{2u} \pm {}^1/_2\rangle$ transitions that become allowed when spin–orbit coupling is included.

Type a transitions, which are predicted to occur below 500 cm^{-1} with our Figure 4 parameters, have not been observed experimentally. In accordance with this, in the dipole length formalism they are predicted to have negligible intensity relative to the other bands. In contrast, the dipole velocity method predicts incorrectly that they will dominate the low-energy spectrum.

Type b low-energy transitions are predicted to have roughly similar spectra relative to the mixed-valence band in the two formalisms. The dipole length calculations predict the lower energy $\varphi_1^0 = |^2B_{2g} \pm {}^1/_2\rangle \rightarrow \varphi_3^0 = |^2B_{1u} \mp {}^1/_2\rangle$ band to be somewhat more intense relative to the mixed-valence band. Both methods predict a very weak $\varphi_1^0 = |^2B_{2g} \pm {}^1/_2\rangle \rightarrow \varphi_5^0 = |^2B_{2u} \pm {}^1/_2\rangle$ transition relative to the mixed-valence band. As we discuss ahead, the two transitions observed experimentally in this region are weak; the intensity of the higher energy of the two appears to be vibronically induced.[10] The dipole length calculations for type b bands again overestimate intensities, much as they do for the mixed-valence band.

In summary, the dipole length calculations reproduce the band shape of the C–T ion somewhat better than the dipole velocity calculations in the region below 10 000 cm^{-1}, but the absolute intensities calculated are much too high. Dipole velocity intensities are closer to those observed with the exception of the very low energy infrared transitions. The question of how best to calculate intensities in molecular systems of this type is an interesting problem that warrants further investigation.

In our figures in this paper, we plot absorption profiles in relative absorbance units only. Calculations were made with the dipole length formalism assuming that the $\varphi_2^0 \rightarrow \varphi_3^0$, $\varphi_4^0 \rightarrow \varphi_5^0$, and $\varphi_1^0 \rightarrow \varphi_6^0$ transitions had equal intensities. As pointed out above, in the dipole length formalism the intensity of the $\varphi_1^0 \rightarrow \varphi_6^0$ transition is diminished somewhat by π bonding. When we correct for this, the bands below 5000 cm^{-1} increase slightly in intensity relative to the mixed-valence band, beyond that shown in our figures.

Calculation of g Values. If we define $|+\rangle$ and $|-\rangle$ as the ground-state Kramers doublet partners that move up and down, respectively, in a magnetic field, then

$$g_x = 2\langle +|(L_x + 2S_x)|+\rangle$$
$$g_y = 2i\langle +|(L_y + 2S_y)|-\rangle$$
$$g_z = 2\langle +|(L_z + 2S_z)|+\rangle \qquad (16)$$

To calculate g values, we obtain the matrix elements of the components of **L** and **S** in our electronic basis of eq 5. We then transform the matrices using the ground-state eigenvectors to obtain ground-state g values. In the calculation of the **L** matrices, two-center terms are dropped as are single-center pyrazine contributions. No explicit orbital reduction factor was used. However, MO formation leads to reduced orbital angular momentum matrix

(16) Moscowitz, A. *Modern Quantum Chemistry, Part III*; Sinanoglu, O. Ed.; Academic Press: London, 1965, pp 31–44.
(17) Schatz, P. N.; Piepho, S. B.; Krausz, E. R. *Chem. Phys. Lett.* **1978**, *55*, 539–542.

Table II. Parameters Used in Figure 4 and Resulting Quantities Calculated with Them

	a	b	c
	Electronic Parameter Used (cm^{-1})		
$\alpha(\pi^*)$	15230	16850	17700
$\epsilon(b_{3u})$	4450	3560	3120
$\alpha(\pi)$	18300	16680	16060
$\epsilon(b_{2g}^*)$	2000	2760	3120
ϵ(tet)	530	750	875
ζ	685	1000	1150
	Resulting Quantities		
$J(b_{3u})$ (cm^{-1})	6617	6027	5699
c_1	0.903	0.923	0.933
c_2	0.429	0.385	0.361
$J(b_{2g})$ (cm^{-1})	4506	5180	5470
d_1	0.954	0.936	0.927
d_2	0.300	0.353	0.374
$g_x(1.346)^a$	1.347	1.351	1.345
$g_y(2.799)^a$	2.756	2.745	2.745
$g_z(2.487)^a$	2.428	2.428	2.421
	Vibronic Parameters Used		
$\lambda_1^{(6)} = 0.7$, $\nu_1 = 800$ cm^{-1}, $\kappa = 1.0$, $\lambda^{PKS} = 1.1$, $\nu_2 = \nu_- = 500$ cm^{-1}			

[a] Experimental values.[18]

elements through the c_1 and d_1 coefficients in the eq 4 MO's.

III. Results

The goal of our calculations is to simulate the mixed-valence absorption profile and calculate the g values of the C–T ion. In addition, we would like to understand the results of Krausz and co-workers that include the region below 6000 cm^{-1}.[10] The set of electronic and vibronic parameters needed to optimize the fit may then be used to understand better the electronic structure and vibronic interactions of the C–T ion and, more generally, the interdependence of vibronic and MO effects in such systems. The experimental g values for the ion are[18]

$$g_x = 1.346 \qquad g_y = 2.799 \qquad g_z = 2.487 \tag{17}$$

The calculated g values are very sensitive to the choice of electronic parameters. They also are affected by vibronic coupling.

Electronic Parameters and the Low-Energy Bands. We estimate the electronic parameters and calculate the absorption profile as discussed earlier, making use of spectroscopic and other experimental data. Figure 4a–c gives the absorption profile for a two-mode calculation in Q_1 and Q_2 for three representative sets of electronic parameters. The parameters used are given in Table II along with the g values, MO coefficients, and J values obtained with them. The three parameter sets reproduce the C–T absorption profile (see Figure 4) and g values (Table II) equally well. They differ, however, in their prediction of the absorption profile in the 1000–4000-cm^{-1} region. The parameter sets illustrated in Figure 4 are not unique; there are a continuum of possible parameter sets that would illustrate cases between parts a and b of Figure 4 and between parts b and c of Figure 4 and would give equally good g values and C–T band absorption profile.

Superimposed on the figures is the room-temperature mixed-valence band from ref 2a. In these and subsequent figures, the spectra were simulated with a Gaussian line shape with a line width of 600 cm^{-1}. The stick spectra give the maxima of the Gaussian curves for individual vibronic lines. The simulated spectra are normalized so that the C–T peak coincides with that of the experimental data. Results are independent of the signs of the λ parameters.

Preference for one of the Figure 4 parameter sets depends largely on the fit of the low-energy results of Krausz et al. Krausz and co-workers have measured the magnetic circular dichroism and the absorption spectra of the C–T ion down to about 1800 cm^{-1}.[10] They observe a very weak electronic absorption band in the 2000–2700-cm^{-1} region and another weak vibronically induced absorption band in the 3200–3600-cm^{-1} region. Both bands are ill-defined. Our earlier discussion suggests that the 2000–2700-cm^{-1} band be assigned to the $b_{1u} \rightarrow b_{2g}^*$ excitation and the 3200–3600-cm^{-1} features be assigned to the $b_{2u} \rightarrow b_{2g}^*$ excitation.

The two excitations above appear as low-intensity bands in the Figure 4 simulations in the 1000–4000-cm^{-1} region; the second band is barely discernible as a high-energy shoulder on the first band. The lower energy band in the simulation arises from the $b_{1u} \rightarrow b_{2g}^*$ excitation while the $b_{2u} \rightarrow b_{2g}^*$ excitation is responsible for the shoulder. These excitations are both orbitally forbidden but become allowed due to spin–orbit coupling; thus, their intensity increases as ζ increases. As we go from part a to c in Figure 4, both of these bands move to higher energy and increase in intensity. The increases in energy of the $b_{1u} \rightarrow b_{2g}^*$ band and the $b_{2u} \rightarrow b_{2g}^*$ shoulder are due largely to increases in the magnitude of $\epsilon(b_{2g}^*)$. The intensity increases result from increases in ζ. Both ζ and ϵ(tet) must be increased as $\epsilon(b_{2g}^*)$ increases in order to obtain acceptable g values. As mentioned earlier, $\epsilon(b_{2g}^*)/\zeta$ and $\epsilon(\text{tet})/\zeta$ ratios must be kept within narrow limits if reasonable g values are to be calculated.

Assignment of the above excitations to the very weak bands observed by Krausz et al. in the same general region supports parameters in the range of those of parts b and c of Figure 4 on energy grounds. These parameters predict somewhat higher relative intensities for these low-energy bands than are observed experimentally. However, as indicated earlier, intensities cannot be calculated for the C–T ion with accuracy. Thus, it is probably best to view even our calculated relative intensities as highly approximate. The $b_{2u} \rightarrow b_{2g}^*$ excitation shows up only as a weak shoulder in our Figure 4 simulations; thus its *allowed* intensity is low enough that it could easily be dominated by vibronically induced intensity involving a mode not included in our calculation. Alternatively, some of the vibronically induced intensity observed experimentally in this region could arise from the parity-forbidden $a_{1g} \rightarrow b_{2g}^*$ and $b_{3g} \rightarrow b_{2g}^*$ excitations that are predicted fairly close in energy to the $b_{1u} \rightarrow b_{2g}^*$ and $b_{2u} \rightarrow b_{2g}^*$ excitations, respectively (see Figure 2). We do not attempt calculation of this vibronically induced intensity.

The Figure 4c parameters have the simplifying feature that $\epsilon(b_{2g}^*) = \epsilon(b_{3u})$, but ζ is somewhat higher in value than the 1000 cm^{-1} usually cited for Ru d electrons. In this respect the Figure 4b parameters are preferred.

Vibronic Parameters. Parts a–c of Figure 4 give results for a two-mode calculation in Q_1 and Q_2 with a constant set of vibronic parameters. As discussed above, the off-diagonal vibronic constant λ^{PKS} for $Q_2 = Q_-^{loc}$ is estimated to be 1.1 for the Creutz–Taube ion with a frequency ν_- of 500 cm^{-1}. We keep λ^{PKS} and $\nu_2 = \nu_-$ constant at these values throughout this paper. As mentioned earlier, when λ^{PKS} has this magnitude, the $Q_2 = Q_-^{loc}$ vibronic coupling has very little effect on the band shape. The effect of Q_3 is even less. Figure 4 does not include Q_3; however, we find that inclusion of $Q_3 = Q_+^{loc}$ in the analogous three-mode calculation using the eq 15 relations makes no discernible difference in our results.

In the two-mode calculation of Figure 4, the band shape is determined almost entirely by vibronic coupling to the molecular mode we designate as Q_1. In Figure 4, the diagonal vibronic constants for $Q_1 = Q_+^{mol}$ of eq 13 are $\lambda_1^{(j)} = 0.35$ for $j = 2$–5 and $\lambda_1^{(6)} = 0.70$ (which corresponds to $\kappa = 1.0$ in eq 13) with $\nu_1 = 800$ cm^{-1}. The effect of variation of κ on the band shape is slight. These values fit the C–T band shape very well except for the high-energy tail of the band. Figures 5 and 6 illustrate how the Q_1 vibronic parameters affect the band shape. Electronic parameters used are essentially those of Figure 4c; however, small adjustments have been made so that the maximum absorption for the simulated and experimental spectra coincide. $\lambda_1^{(6)}$ must be kept low to reproduce the asymmetry of the C–T band. Values of both $\lambda_1^{(6)}$ and ν_1 affect the width as illustrated in Figures 5 and 6, respectively.

It is tempting to choose the $\nu_1 \approx 1000$ cm^{-1} results as the best fit since Figure 6c best reproduces the high-energy tail of the C–T

(18) Fürholz, U.; Bürgi, H.-B.; Wagner, F. E.; Stebler, A.; Ammeter, J. H.; Krausz, E.; Clark, R. J. H.; Stead, M. J.; Ludi, A. *J. Am. Chem. Soc.* **1984**, *106*, 121–123.

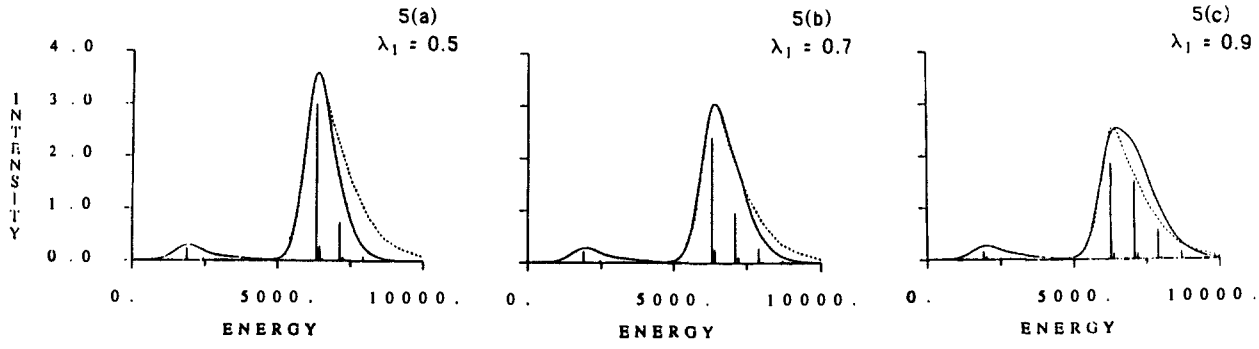

Figure 5. Dependence of the two-mode Figure 4c absorption profile at 298 K on $\lambda_1^{(6)}$. Other parameters are those of Figure 4c except that small adjustments in the electronic parameters have been made in a and c to ensure that the maximum absorptions for the simulated and experimental spectra are aligned. The dashed curve is the experimental absorption spectrum from ref 2a.

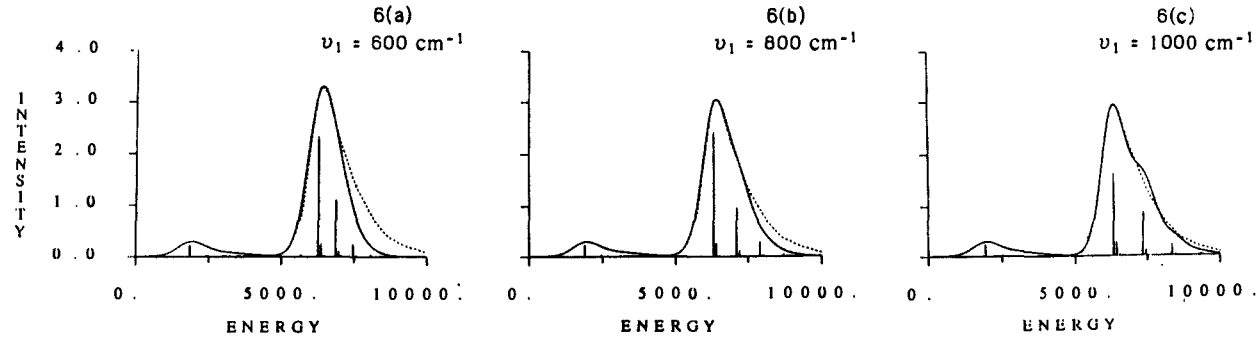

Figure 6. Dependence of the two-mode Figure 4c absorption profile at 298 K on ν_1. Other parameters are those of Figure 4c except that small adjustments in the electronic parameters have been made in a and c to ensure that the maximum absorptions for the simulated and experimental spectra are aligned. The dashed curve is the experimental absorption spectrum from ref 2a.

absorption profile. But for reasons that we outline below, it is unlikely that the origin of the high-energy tail, or of the weak shoulder that is apparent in some C–T ion spectra, is associated with a totally symmetric vibrational mode such as Q_1. The shoulder, which probably has the same origin as the high-energy tail, is most clearly seen in the deuterated spectra of Figure 4 of Krausz and Ludi[19] and in the high-pressure spectra of Hammack et al.[12] The weak shoulder appears to fall 600–650 cm^{-1} from the peak in the deuterated spectrum,[19] while in the high-pressure spectra it falls farther from the peak (>900 cm^{-1}), with the energy separation decreasing as the pressure increases.[12]

The data of Krausz and Ludi[19] are of particular interest to us here. The magnetic circular dichroism (MCD) of the C–T ion mixed-valence band given in Figure 5 of their paper clearly shows a diminished tail relative to the absorption spectrum. The high-energy tail also shows linear polarization properties different from those of the rest of the band. If the high-energy tail were due to a totally symmetric mode (such as our Q_1), the MCD C term band shape should mimic that of the absorption; it should also have the same polarization properties as the no-phonon line of the band. Krausz and Ludi suggest that the high-energy shoulder could arise from vibronic structure associated with a non totally symmetric vibration or from another electronic transition. The C–T ion ESR data[18] appear to rule out the presence of another electronic transition in this region that involves our eq 5 basis states, and there are no other likely candidates. Moreover, Krausz and Ludi state that their deuteration results indicate that the structure is most likely due to a non totally symmetric vibrational sideband system associated with the same electronic transition that gives rise to the rest of the band shape.[19]

On the basis of the experimental evidence cited above, we conclude that the high-energy tail (which we take to include the weak shoulder, if present) of the C–T ion mixed-valence band arises from vibronic interactions with a non totally symmetric mode not included in our model. If one fits the part of the C–T absorption profile that Krausz and Ludi find to have uniform MCD and polarization properties, parameters such as those in part a or b of Figure 6 appear to give the best fit.

Since $Q_1 = Q_+^{mol}$ is an even-parity molecular mode, it is appropriate to look at Raman data for the C–T ion to estimate its frequency. The data[20] suggest two possibilities: ν_{6a} = 701 cm^{-1} and ν_{Ru-pyr} = 328 cm^{-1}. The 328-cm^{-1} mode has no pyrazine or Ru hexaammine analogue. While it is a molecular mode, its frequency is too low to give a band shape anything like that of the C–T band. On the other hand, the ν_{6a} frequency is in approximately the right range (see Figure 6). Moreover, since ν_{6a} for the C–T ion is over 100 cm^{-1} higher in energy than ν_{6a} in pyrazine, it is quite likely a molecular mode: that is, it involves significant contributions from parts of the molecule other than the pyrazine ring. We want a mode whose motion connects the bond lengths before and after the $b_{3u}(d,\pi^*) \rightarrow b_{2g}^*(d,\pi)$ excitation. The ν_{6a} mode of pyrazine does this for the analogous MO's on pyrazine. We assume that in the C–T ion ν_{6a} is a molecular mode that also includes some Ru–N(pyr) stretch.

One further possibility is that the 328- and the 701-cm^{-1} modes are both vibronically active. We explored this possibility in a three-mode calculation using Q_1, Q_2, and Q_4, where Q_4 is now a molecular mode with vibronic matrix elements analogous to Q_1 but with a different frequency and OVC. Equation 13 applies but with the subscript 1 replaced with 4. Results are given in Figure 7 for the Figure 4c parameters with ν_4 = 328 cm^{-1}, κ = 1.0, and $\lambda_4^{(6)}$ = 0.4, 0.8, and 1.0. We see that, except for very small $\lambda_4^{(6)}$ values, additional coupling to this mode leads to a broader band than is observed.

Variatons in vibronic parameters affect the g values, with g_x showing the greatest sensitivity in all cases. However, for small variations in these parameters such as those illustrated in the figures, the effects are small ($\leq \pm 0.05$ unit). Larger changes in vibronic parameters can, however, have a more dramatic effect on the g values; for example, if the Figure 4c parameters are used but with λ^{PKS} increased from 1.1 to 2.0, g_x decreases from 1.345 to 1.116.

(19) Krausz, E.; Ludi, A. *Inorg. Chem.* **1985**, *24*, 939–943.

(20) Strekas, T. C.; Spiro, T. G. *Inorg. Chem.* **1976**, *15*, 974–976.

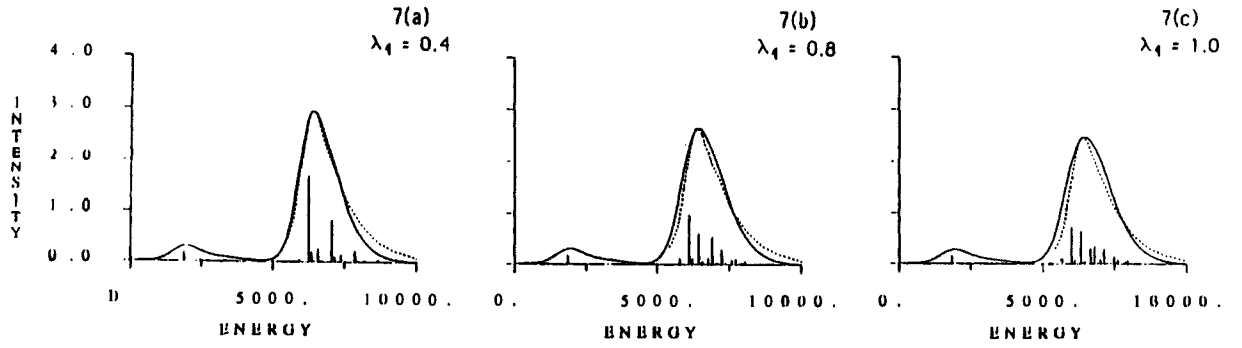

Figure 7. Three-mode simulated absorption profiles at 298 K. The third mode is ν_4 = 328 cm^{-1} with $\lambda_4^{(6)}$ values as indicated. Other parameters are those of Figure 4c. The dashed curve is the experimental absorption spectrum from ref 2a.

Comparison with the Work of Ondrechen and Co-workers. A comparison of our treatment with the recent results of Ondrechen et al.[4e-g] is of interest. The authors[4f] have performed spin-polarized MO calculations on the C–T ion and have also calculated g values[4e,f] using a basis of orbitals we label as $a_g(d)$, $b_{3g}(d)$, $b_{2g}(d)$, and $b_{3u}(d,\pi^*)$ in our eqs 2–4 and the $b_{3u}{}^*(\pi^*,d)$ MO that we do not give explicitly. Calculated ground-state MO energy gaps were used to obtain the energies of the basis orbitals. The energies for these five orbitals were then equated to expressions given for the same quantities (see eqs 12–16 in ref 4f) in terms of the parameters α and J (which are analogous to our $\alpha(\pi^*)$ and $J(b_{3u})$ parameters) and tetragonal (D) and rhombic (E) splitting parameters. These equations were solved for the four parameters α, J, D, and E, which were then used along with the spin–orbit coupling constant ξ in the ESR calculation. The value of ξ was obtained by fitting the experimental ESR data.

While the Zhang, Ko, and Ondrechen[4f] MO calculations provide valuable information, we see several difficulties in the way they have applied their MO results.

First, while MO calculations of the type carried out by the authors may give the correct MO orders and are useful in getting an overall feel for the transitions of interest, they give only rough estimates of the energies of closely spaced MO's such as the ones relevant here to the ESR. For example, in this case the MO calculation predicts the mixed-valence band peak at 5700 cm^{-1} while it occurs experimentally at around 6400 cm^{-1}. While our method is admittedly empirical, it does show what magnitude interactions are required to reproduce the experimental data and describes the physical origin of those interactions in simple terms.

Second, we are puzzled by the authors' introduction of the rhombic splitting parameter E in eqs 12–16 of ref 4f. They use the E parameter in the typical crystal field manner. Yet it seems clear to us that the "rhombic" splitting in the C–T complex arises physically from MO formation of Ru symmetry orbitals with the π and π^* pyrazine orbitals to give the b_{2g} and b_{3u} MO's. Thus, in our MO approach the rhombic splittings are parameterized by $J(b_{3u})$ and $\alpha(\pi^*)$ for the b_{3u} MO's and by $J(b_{2g})$ and $\alpha(\pi)$ for the b_{2g} MO's: these give rise to the Figure 2 energy shifts of $-\epsilon(b_{3u})$ and $\epsilon(b_{2g}{}^*)$, respectively. The crystal field rhombic splitting parameter E is essentially replaced by $-\epsilon(b_{2g}{}^*)$ in our treatment. (Likewise, our ϵ(tet) parameter replaces $D - {}^1/_2E$.) Ondrechen and co-workers recognize the role of the $b_{3u}(\pi^*)$ pyrazine MO in giving rise to the $b_{3u}(d)$ energy shift, but they fail to acknowledge the role of the $b_{2g}(\pi)$ pyrazine MO in producing an analogous $b_{2g}(d)$ energy shift. Instead they turn to the E parameter.

The E value of −2000 cm^{-1} that Ko, Zhang, and Ondrechen[4e] obtain from their MO calculation via eqs 12–16 of ref 4f is actually a measure of the extent of π bonding in the $b_{2g}{}^*(d,\pi)$ MO; in fact, their parameters[4e] of E = −2000 cm^{-1}, D = −330 cm^{-1}, and ξ = 690 cm^{-1} translate into $\epsilon(b_{2g}{}^*)$ = 2000 cm^{-1}, ϵ(tet) = 670 cm^{-1}, and ζ = 690 cm^{-1} in our notation—close to our Figure 4a parameters (see Table II). This $\epsilon(b_{2g}{}^*)$ value of 2000 cm^{-1} shows that π bonding in the $d_{2g}(d,\pi)$ MO plays an important role in Ondrechen et al.'s treatment, a result ignored by the authors. We argue that π bonding is even greater than this: parameter sets such as those of Figure 4b,c give better fits to the data. As we point out, the $\epsilon(b_{2g}{}^*)/\zeta$ ratio must be kept within narrow limits if reasonable g values are to be calculated; hence, low $\epsilon(b_{2g}{}^*)$ values lead to unrealistically low ζ values. Thus, the spin–orbit coupling constant Ondrechen et al. obtain in their fit, 690 cm^{-1},[4e] is quite a bit lower than the 1000 cm^{-1} commonly cited for Ru 4d orbitals. As discussed above, other experimental data[9,10] also support a larger π-bonding interaction than that implied by Ondrechen et al.'s MO results.

In ref 4g Ondrechen et al. present vibronic calculations for the C–T ion. Their method uses a three-site, three-mode model Hamiltonian that is later extended to five modes. Thus, their electronic basis is *very much* simplified and the *only* electronic interaction included is that giving rise to the $b_{3u}(d,\pi^*)$ and $b_{3u}{}^*(\pi^*,d)$ MO's. In contrast, we use the *same* electronic basis and interactions for our vibronic calculations as we do for our ESR and electronic absorption spectrum calculations. Thus, for example, we are able to study the effect of vibronic coupling on the ESR. Ondrechen et al.'s vibrational modes are localized in specific sites or bonds. We, however, look into the effect of molecular modes as well as local modes and consider how the magnitudes of the orbital vibronic constants that govern vibronic coupling are related to the MO's involved. Thus, in comparison with Ondrechen and co-workers, we tie the electronic and vibronic parts of our calculations much more closely together. Again our treatment is empirical and uses simple physical arguments to explain parameter magnitudes. We do not make the Born–Oppenheimer approximation so our vibronic results are more exact; however, since vibronic coupling in the C–T complex is relatively weak, this difference should not be important in this case.

IV. Conclusions

We present calculations of the band shape and g values of the C–T ion using a vibronic coupling model with a molecular orbital basis. Parameters used are estimated from experimental data. The analysis supports the conclusion that the ion is a delocalized mixed-valence system with the mixed-valence band arising from the $b_{2g}{}^*(d,\pi) \rightarrow b_{3u}(d,\pi^*)$ excitation. Both π^* back-bonding in the $b_{3u}(d,\pi^*)$ MO and π bonding in the $b_{2g}{}^*(d,\pi)$ MO are significant. The latter is required to explain not only the solvent dependence as pointed out by Creutz and Chou[9] but also the low-energy spectrum measured by Krausz et al.[10] and the g values. The large rhombic splitting parameter used to fit the g values in earlier analyses of the C–T ESR spectrum is simply a manifestation of the sizable π-bonding interaction that gives rise to the $b_{2g}{}^*(d,\pi)$ MO.

It is not possible to precisely specify all the relevant parameters for the system because the bands below 6000 cm^{-1} in the experimental spectra are ill-defined. Nevertheless, parameters in the range of those used for Figure 4b,c and tabulated in Table II are good approximations.

Our analysis of the C–T ion supports the conclusion that the mixed-valence band shape arises primarily from coupling to a molecular mode Q_1^{mol} whose motion connects the bond lengths before and after the $b_{3u}(d,\pi^*) \rightarrow b_{2g}{}^*(d,\pi)$ excitation. Our fits suggest the frequency of this mode is in the 600–800-cm^{-1} range with a vibronic coupling parameter $\lambda_1^{(6)}$ equal to 0.70. The frequency best matches that of the 701-cm^{-1} mode observed in the C–T ion Raman spectrum;[20] the 328-cm^{-1} Raman mode[20] does

not appear to be active, either by itself or in combination with this mode. The size of $\lambda_1^{(6)}$ reflects the narrow width of the mixed-valence band. The small value can be explained by cancellation effects in contributions to the b_{2g}* and b_{3u} OVC that contribute to $\lambda_1^{(6)}$—see the discussion preceding eq 11. The data of Krausz and Ludi[19] strongly suggest that the origin of the high-energy tail of the mixed-valence band (and of the weak shoulder, if present) arises from non totally symmetric vibronic interactions not included in our model.

The parameter λ^{PKS} is a measure of the extent of vibronic coupling to $Q_2 = Q_-$, the active mode in the PKS model.[3] Following Wong and Schatz, we estimate λ^{PKS} from the difference in bond lengths between the oxidized and reduced forms of the metal ion centers to be 1.1.[11] For the C-T ion when λ^{PKS} has this magnitude, vibronic coupling to Q_2 has very little effect on the band shape.

While electronic parameters have a large effect on band positions and g values, they have no effect on the band shape of individual bands. However, vibronic parameters *do* have a noticeable effect on the g values—particularly on g_x. The effect is, however, small for changes in these parameters of the magnitude of those illustrated in Figures 5-7.

Our analysis in this paper is directed specifically at the C-T ion. However, the methods used are presented in a general form and can be easily applied to other ions.

Acknowledgment. This work was supported under National Science Foundation Grants CHE8604470 and RII-8600354 and in part under Grant CHE8400423. Most of the calculations were made possible by a grant of time by the Pittsburgh Supercomputing Center. I also acknowledge many useful discussions with Professor Paul N. Schatz and the able assistance of Kelly Lenz and Suzanne Szak with the computer programming and of Wei Tang with the figures. Thanks also go to the University of Virginia for its hospitality during my year there under the NSF/VPW program.

Electric Field Induced Intramolecular Electron Transfer in Spiro π-Electron Systems and Their Suitability as Molecular Electronic Devices. A Theoretical Study

Abbas Farazdel, Michel Dupuis,* Enrico Clementi, and Ari Aviram[†]

Contribution from IBM Corporation, Data Systems Division, Department 48B/MS 428, Kingston, New York 12401. *Received October 30, 1989*

Abstract: Intramolecular electron-transfer properties and their dependence on an external electric field are studied for a typical rigid spiro $\pi-\sigma-\pi$ molecular cation by ab initio MO methods. Our study indicates that the molecule exhibits characteristics appropriate for molecular device applications. Formulas and algorithms are presented for the calculation of the ubiquitous electron-transfer matrix element.

The direction of research in modern electronic technology is leading toward the development and fabrication of ever more miniature electronic components. At the same time, there have been significant advances on both theoretical[1-3] and experimental[2] fronts supporting the idea that it may be possible to develop devices of the size of individual molecules, i.e., molecular electronic devices. A class of molecules originally proposed by Aviram and Ratner[1] and later expounded by Aviram[3] as strong candidates for molecular electronic devices is of the $\pi-\sigma-\pi$ type. These molecules consist of a conductor (C) and a proconductor (PC)[4] π-electron moiety separated by a rigid σ bridge. In order for such a molecule to function as a device, the C site should effectively be insulated from the PC site[3] (see below). This is achieved by having a spirocycloalkane as the σ bridge, making the plane of the C unit perpendicular to that of the PC unit. A group of molecules that meet these requirements is exemplified by the molecular cation **1**:

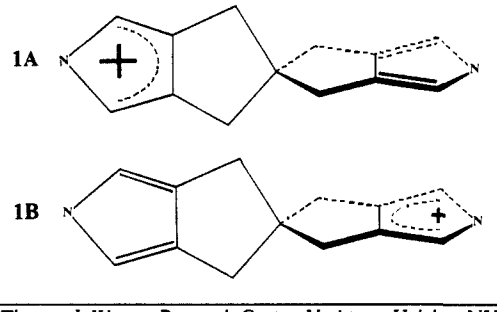

Here **1A** and **1B** represent two possible localized electronic structures of **1**. We refer to **1A** as a left-localized or an A state and to **1B** as a right-localized or a B state.

Qualitatively, **1** and other molecules of this type can be looked upon as a double-well potential for an electron that can hop back and forth between the two wells at some characteristic frequency, which depends on the height and the shape of the potential barrier.[5] Such a two-state molecule conceivably can serve as a binary system in which one state represents "on" and the other represents "off". In this case the two minima should be separated by a sufficiently high barrier corresponding to a small characteristic frequency, so that neither tunneling nor thermal fluctuations can unintentionally switch one state to the other. Only by an external control

[†]IBM Thomas J. Watson Research Center, Yorktown Heights, NY 10598.

(1) Aviram, A.; Ratner, M. A. *Chem. Phys. Lett.* **1974**, *29*, 277; *Bull. Am. Phys. Soc.* **1974**, *19*, 341. Aviram, A. IBM Research Report RC 9953 (No. 43939) March 28, 1983.

(2) Carter, F. L., Ed. *Molecular Electronic Devices*; Marcel Dekker, Inc.: New York, 1982; *Molecular* Electric Devices *II*; Marcel Dekker, Inc.: New York, 1987. Third International Symposium on Molecular Electronic Devices, Washington DC, October 1986; Roland Etvos Physical Society, Satellite Symposium on Molecular Electronics, Budapest, Hungary, August 1987.

(3) Aviram, A. *J. Am. Chem. Soc.* **1988**, *110*, 5687.

(4) The "conductor" (C) form of a compound has a partially filled highest occupied molecular orbital (HOMO) and therefore a partially filled conduction band in the solid state. On the other hand, the proconductor form of the same compound has a fully occupied HOMO and is nonconductive. The C and PC forms are related to each other by either oxidation or reduction as the case may be. For more details, see: Reference 3, and further references therein.

(5) Merzbacher, E. *Quantum Mechanics*; 2nd ed.; John Wiley & Sons: New York, 1970. Eliasson, B.; Staley, S. W. *Prepr.—Am. Chem. Soc., Div. Pet. Chem.* **1985**, *30*, 620.

0002-7863/90/1512-4206$02.50/0